Polymorphic Crystallization and Melting−Recrystallization Behavior of Poly(3-hydroxypropionate)

Bo Zhu,[†] Yong He,[†] Naoki Asakawa,[†] Naoko Yoshie,[‡] Haruo Nishida,[§] and Yoshio Inoue*,[†]

Department of Biomolecular Engineering, Tokyo Institute of Technology, Nagatsuta 4259-B-55, Midori-ku, Yokohama 226-8501, Japan; Institute of Industrial Science, The University of Tokyo, Komaba 4-6-1, Meguro-Ku, Tokyo 153-8505, Japan; and Molecular Engineering Institute, Kinki University, 11-6, Kayanomori, Iizuka, Fukuoka 820-8555, Japan

Received March 13, 2005; Revised Manuscript Received May 15, 2005

ABSTRACT: Using wide-angle X-ray diffraction, high-resolution solid-state ^{13}C NMR (SNMR), attenuated total reflection infrared (ATR/IR), and Fourier transform infrared (FTIR) spectrometry, we investigated the crystalline structure and morphology of melt-crystallized poly(3-hydroxypropionate)s (PHPs). The melt-crystallization of the β-form crystal and that of the γ-form crystal are found to be favored respectively thermodynamically at higher temperature and kinetically at lower one. In addition, the PHPs with higher molecular weight more readily crystallize into the γ-form crystal. In this way, the polymorphism leads to the bimodal growth behavior for PHP spherulites, attending by a discontinuously temperature-dependent morphology phenomenon. PHP chains take on a similar conformation (the trans) in both type crystals but are packed with different efficiency. In the γ-form, the tighter packing of the atoms along the a axis make the adjacent chains strongly interact with each other, resulting in the crystal field splitting. The corresponding splitting of IR absorption distinguishes the γ-form from the β-form, which endows us with the capability to in-situ monitor the structure evolution during the crystallization and melting. In the crystallization, PHP chains are always crystallized into the γ- and β-form crystal at a constant ratio, which value depends on the temperature. In the melting, only the γ-form crystal can be reorganized via the melting−recrystallization, resulting in the enrichment of the γ-from in the recrystallized phase and the split melting of the two forms for the γ-rich sample.

Introduction

Poly(hydroxyalkanoates) (PHAs) are found as endogenous carbon reserves in bacteria (e.g., poly(3-hydroxybutyrate), PHB) and as chemosynthetic materials. PHAs, especially bacterial ones, attract much attention from the industry and the researchers,[1−6] as their good biodegradability offers an effective route to alleviate the environmental concerns. Normally, the physical property, biodegradability, and processing of PHAs are expected to quite depend on their crystalline structures. However, the polymorphism of biodegradable PHAs has not received the attention it deserves yet. So far, only limited research results can be obtained on crystal modifications in poly([*R*]-3-hydroxybutyrate) (PHB),[7,8] poly(L-lactide),[9,10] and poly(3-hydroxypropionate) (PHP),[11−14] and few systematical researches have been carried out to investigate the polymorphism of PHAs. The poor understanding of polymorphic behavior of PHAs prevents us to clarify the effect of polymorphism on the biodegradation, which is recently concerned by biologists and polymer scientists.

Poly(3-hydroxyalkanoate)s (P3HAs) are based on a 3-hydroxypropionate (HP) skeleton in terms of chemical structure. It is well-known that the chain conformations of P3HAs are quite related to their skeleton structures. Conformational analyses predict that almost all P3HAs will have identical conformations in the crystalline state, i.e., 2_1 helix.[15] Also, the planar zigzag conformation is energetically allowed for PHP-based polyesters, with low-energy barriers separating the two conformations.[16] Because of the similarity in the chemical structure and the conformation in crystalline state, the research on the polymorphism of PHP possibly sheds light on the understanding of crystallization and biodegradation of P3HAs.

PHP is known to show a complex polymorphic behavior depending on the conditions of sample preparation.[11−14] The PHP backbones can be regularized into the 2_1 helix conformation in the α-form (a fiber repeat distance of 0.702 nm[12]) and the all-trans conformation in the β-form (a fiber repeat distance of 0.482[12] or 0.477 nm[11]) by drawing the cast films at different temperature or to the all-trans conformation in the γ-form (a fiber repeat distance of 0.493 nm[13]) in the solution-grown lamellar. The orthorhombic unit cell dimensions of the β form is a = 0.773 nm, b = 0.448 nm, and c = 0.477 nm,[11] while the two-chain, C-faced, orthorhombic unit cell of the γ-form has dimensions of a = 0.700 nm, b = 0.490 nm, and c = 0.493 nm.[13]

The previously reported crystal modifications for PHP are all found in the highly stretched fiber or the solution-grown lamellar. Until now, there still remain challenges whether these crystal modifications can be crystallized spontaneously during melt-crystallization free from strain. It is of scientific interest to understand their different thermal accessibility and growth kinetics at a specific temperature with considering their crystalline structures and chain conformations. In application, it is quite important to control the polymorphism for optimizing their properties and production process. In addition, the research of polymorphism in the biodegradable polymer with polymorphic crystals also allows

[†] Tokyo Institute of Technology.
[‡] The University of Tokyo.
[§] Kinki University.
* To whom all correspondence should be addressed: Tel +81-45-924-5794, Fax +81-45-924-5827, e-mail yinoue@bio.titech.ac.jp.

10.1021/ma050534q CCC: $30.25
Published on Web 06/28/2005

us to reveal the relationship between the structure or chain conformation and biodegradability. It can be predicted that the polymer chains, even though they share the common chemical structure, may have different biodegradabilities. This is not only due to difference in the size of crystal and the degree of crystallinity but also possibly to that in the spatial orientation and packing of polymer chains in the polymorphic crystal lattice.

In the present study, we report a detailed and systematic research about the polymorphic crystallization and the melt-recrystallization of PHPs, part of which has been simply referred in our most recent rapid communication work.[17] The effects of crystallization condition and the molecular weight on the crystalline structure and the chain conformations of PHP are investigated by X-ray diffraction, the attenuated total reflection infrared (ATR/IR) spectrometry, the Fourier transform infrared (FTIR) spectrometry, and high-resolution solid-state ^{13}C NMR techniques. Moreover, with combining the differential scanning calorimetry (DSC), the time-resolved FTIR is used to monitor the polymorphic behavior of PHP during the crystallization and the melting.

Experimental Section

Materials. Three kinds of chemosynthesized PHPs (PHP18K: number-average molecular weight $M_n = 1.8 \times 10^4$, $M_w/M_n = 2.48$; PHP23K: $M_n = 2.3 \times 10^4$, $M_w/M_n = 1.20$; PHP70K: $M_n = 7 \times 10^4$, $M_w/M_n = 2.03$) were kindly supplied by Tokuyama Co. (Japan) and purified from chloroform solution by precipitation in *n*-heptane.

Preparation of PHPs with Different Crystal Forms. Film samples for X-ray, solid NMR, and ATR/IR analyses were compression-molded under 5 MPa at 130 °C for 3 min (containing 1.5 min of postannealing without pressure), then quenched to a desired temperature, and annealed for a time to generate polymorphic crystalline phase. Similar thermal treatments were also used to prepare the melt-crystallized polymorphic samples in the POM, DSC, and in-situ FTIR measurements but without pressure loading. In addition, the chloroform solution of PHP70K (10 mg/mL) was cast on the Teflon dish to produce the pure γ-form crystal at 30 °C.

Analytical Procedures. The measurements of wide-angle X-ray diffraction (WAXD) were carried out on a Rigaku RU-200 (Rigaku Co., Tokyo, Japan), working at 40 kV and 200 mA, with Ni-filtered Cu Kα radiation ($\lambda = 0.154\ 18$ nm). Scans were made between Bragg angles of 5−60° at a scanning rate of 1° min^{-1}.

The CP/MAS ^{13}C NMR spectra were registered on a JEOL GSX-270 spectrometer operating at 270.1 MHz for ^1H and 60.8 MHz for ^{13}C. Typical NMR experimental conditions were as follows: 90° pulse length, 5.5 μs; contact time, 1 ms; recycle delay, 5 s; ^1H decoupling field strength, 57 kHz; MAS frequency rate, 5 kHz. ^{13}C chemical shifts were externally referenced to the methyl carbon resonance of hexamethylbenzene at 17.36 ppm.

The spherulite growth was followed by an Olympus BX90 polarizing microscope (Olympus Co., Tokyo, Japan) with a dry nitrogen gas purge. Microphotographs were recorded with a FUJIX digital camera HC-2500 3CCD. The temperature dependence of the spherulite growth rate (G) was measured via following the spherulite radius (r) either in isothermal condition or under cooling.[18]

Both ATR/IR and the transmission FTIR measurements were carried out on AIM-8800 (Shimadzu Co., Japan), an automatic infrared microscope. With employing the attenuated total reflection (ATR) technique, the ATR/IR spectra with an accumulation of 512 scans were collected at 30 °C by coadding 512 scans. The transmission FT-IR spectra with an accumulation of 16 scans were in situ registered during the whole crystallization of PHPs and the subsequent heating at a constant rate of 1 °C/min. Both IR spectra are registered at a resolution of 2 cm^{-1}.

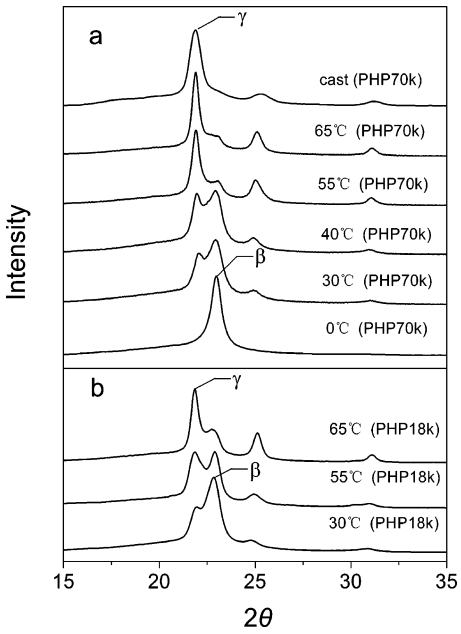

Figure 1. X-ray diffraction profiles of (a) PHP70Ks melt-crystallized at 0, 30, 40, 55, and 65 °C and cast PHP70K, and those of (b) PHP18Ks melt-crystallized at 30, 55, and 65 °C.

The melting of the polymorphic PHPs was also observed by a Perkin-Elmer DSC instrument (Pyris Diamond). The scales of temperature and heat flow at different heating rates were carefully calibrated using an indium standard with nitrogen purging. The samples between 5 and 6 mg were heated at a constant rate (10 or 1 °C/min).

Results

Temperature-Dependent Polymorphism. Crystalline structures and conformations of the PHPs were investigated by the X-ray diffraction and the solid-state ^{13}C NMR.

i. X-ray Diffraction. X-ray diffraction profiles of the cast and melt-crystallized PHP70Ks and those of melt-crystallized PHP18ks are shown in parts a and b of Figure 1, respectively. The PHP70K isothermally crystallized at 0 °C shows one main diffraction peak at 22.9°, which is assigned to the reflection of the β-form.[11] In contrast, the PHP70K isothermally crystallized at 65 °C shows very different diffraction, i.e., one strong and three weak peaks at Bragg angles 22.1°, 22.9°, 25.4°, and 31.5°. Upon employing the Bragg diffraction theory, the experimental spacing values were calculated to be 0.402, 0.351, 0.388, and 0.284 nm, respectively. It is found, except for that of the diffraction at 22.9°, the experimental spacing values are indicating the presence of the γ-form crystal.[13] The diffraction at 22.9° cannot be observed in the typical diffraction of the pure γ-form, which should be arisen from the residual β-form crystal. The pure γ-form crystal can be obtained by casting the chloroform solution of PHP70K at 30 °C. Moreover, it is also noted that the PHP70Ks crystallized in the 30−65 °C region show both kinds of characteristic diffraction peaks, indicating the coexistence of β- and γ-form crystal. The intensity of the diffraction from the β-form crystal decreases while that from the γ-form crystal increases with increasing the crystallization temperature (T_c), suggesting the favored growth of the γ-form crystal at higher temperature. Thus, the γ-form crystal is possibly thermally more stable than the β-form

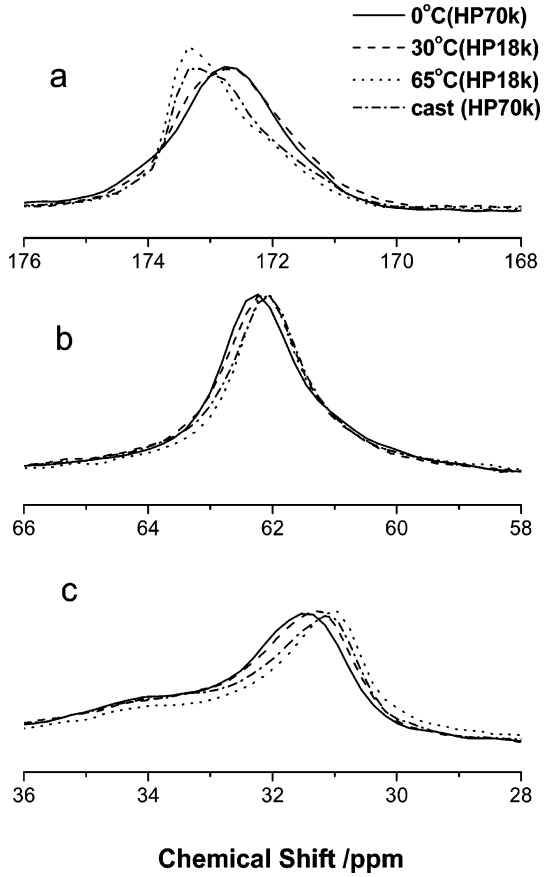

Figure 2. Solid-state ^{13}C NMR CP/MAS resonances of (a) carbonyl group, (b) βCH_2 and (c) αCH_2 for PHP70K melt-crystallized at 0 °C, PHP18Ks melt-crystallized at 30 and 65 °C, and cast PHP70K.

Table 1. ^{13}C Chemical Shift Values of PHP in Various Phases

		chemical shifts (ppm)[a]		
crystal type	sample	carbonyl	βCH_2	αCH_2
β	HP70K (0 °C)[b]	172.8	62.2	31.5
β-rich	HP18K (30 °C)	172.6	62.2	31.3
γ-rich	HP18K (65 °C)	173.4	62.0	31.2
γ	HP70K (casting)[c]	173.4	62.0	31.0

[a] The error in chemical shifts is ±0.2 ppm. [b] Melt-crystallized temperature. [c] Casting with $CHCl_3$.

crystal. The X-ray diffraction profiles of the melt-crystallized PHP18ks are also shown in Figure 1b to evaluate the effect of molecular weight (MW) on the polymorphism. The temperature-dependent polymorphism of PHP18K is similar to that of PHP70K. Nevertheless, at the same T_c, the molecular chains of PHP18Ks are more readily crystallized into the β-form crystal than those of PHP70Ks, suggesting the lower MW would favor the formation of the β-form crystal, and vice versa.

ii. Solid-State ^{13}C NMR Spectroscopy. In Figure 2 are shown the CPMAS ^{13}C NMR spectra of the samples with pure β-form (PHP70K crystallized at 0 °C), β-rich form (PHP18K crystallized at 30 °C), γ-rich form (PHP18K crystallized at 65 °C), and pure γ-form (cast PHP70K). The spectra of the β- and γ-forms are quite similar except for the chemical shift of the carbon in the C=O group. In Table 1 are shown the ^{13}C chemical shift values. Almost no difference between the β- and γ-form crystals can be detected in the chemical shifts of α- and β-carbon with respect to the carbonyl group,

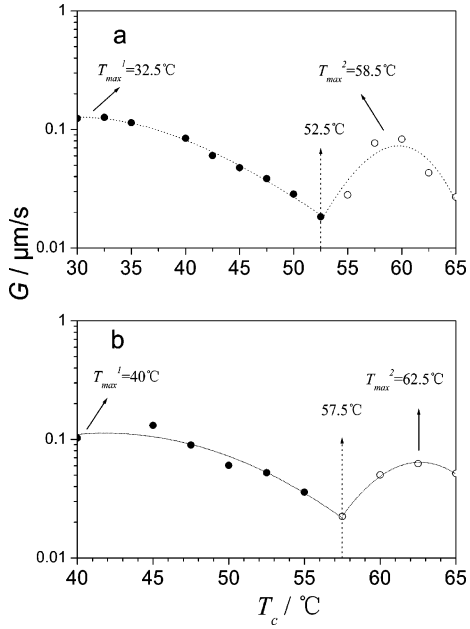

Figure 3. Isothermal radial growth rate of spherulites in (a) PHP18Ks and (b) PHP23Ks as a function of crystallization temperature.

suggesting that the $-C(O)-CH_2-CH_2-O-$ segment takes on a similar conformation in both forms.[19] Furthermore, a difference of about 0.7 ppm can be distinguished in the chemical shift of C=O groups between two kinds of crystals, which should reflect their difference in the chain packing rather than that in the chain conformation, as discussed later.

Multiple Spherulite Morphology and Unique Growth Kinetics. In general, the difficulty in nucleation at low undercooling and the poor diffusivity at high undercooling endure macromolecules with a single bell-shaped growth dependence on the temperature.[20,21] Nevertheless, in the case of PHP, its growth behavior is very unusual. In Figure 3a, the temperature dependence of the growth rates (G) is shown for the PHP18K. Obviously, the G value shows a bimodal temperature dependence, i.e., passes through two maxima (at 58.5 and 32.5 °C) with undercooling. One may argue that the unique spherulite growth would result from the wide MW distribution of the PHP18K (2.48) on the basis of the MW-dependent crystallizability and possible phase segregation. Thus, the PHP23K, which has a MW similar to the PHP18K but a much narrower MW distribution (1.2), is used to further evaluate the growth kinetics. As shown in Figure 3b, the G value of the PHP23K similarly depends on the temperature, reaching two maxima at 62.5 and 40 °C. Two G maxima are separated by a minimum at 57.5 °C, which is 5 °C higher than that for PHP18Ks.

To further confirm the bimodal dependence of G on the temperature, an alternative method, the nonisothermal procedure suggested by Chen and Chung,[18] was used here. It allows a measurement of G over a rather wider temperature range using one sample. Thus, the difference in thickness and other experimental conditions can be excluded from the factors affecting the growth kinetic and the spherulite morphology. A slow cooling rate of 1 °C/min was used to reduce the risk of forming thermal gradient in the direction normal to the sample surface. In Figure 4a is shown the plot of the spherulite radius as a function of temperature for the

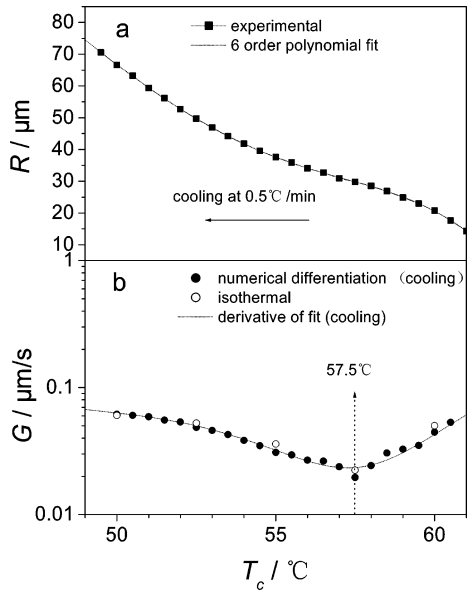

Figure 4. (a) Radius of spherulite in PHP23K cooled from 130 °C at 1 °C/min as a function of temperature. (b) Radial growth rate calculated by taking the first derivative of (a) as a function of temperature, in comparison with that measured during isothermal crystallization.

PHP23K. The growth rates are calculated by taking the first derivative of the r vs T plot. The first derivative is calculated by two methods, i.e., the direct numerical differentiation,[22,23] and that based on the polynomial fitting.[18] The latter method uses a polynomial function with order of 6 to curve-fit the r vs T plot and then differentiates the polynomial function to obtain the G value. In Figure 4b is shown the temperature dependence of G for the PHP23K spherulite growing under cooling. That for the PHP23K spherulite growing isothermally is also included in Figure 4b for a comparison. Obviously, almost no difference can be distinguished between the two G curves.

The morphology is also compared among polymorphic spherulites for the PHP23K and the PHP18K under crossed polars. Despite the temperature, all isothermally grown spherulites exhibit a sheaflike texture aligning radially and a negative birefringence as determined by using a red one-wavelength plate (not shown). Normally, it is reasonable to expect the spherulite structure and texture continuously changes from a coarse texture to a compact one with the decrease of T_c. However, in the case of PHP23K and PHP18K, the texture dependence on T_c is not continuous and thus is unique. In the high-temperature region, being converse to the normal case, the texture with a somewhat distorted Maltese cross became coarser and more opened with the decrease of the temperature, while in the low-temperature region, the texture with a pronounced Maltese cross maintained a similar compact structure despite the change of the temperature. The critical temperature at which the minimum growth rate can be reached between the two maximum ones is found to define the two temperature regions (i.e., 57.5 and 52.5 °C for PHP23K and PHP18K, respectively). The discontinuous change of the texture can be more clearly observed in Figure 5, which describes the developing of spherulite morphology in PHP23ks under cooling. Obviously, the spherulite texture "jumps" from a coarse texture to a compact texture when the temperature passes 57.5 °C, while it almost persists similar at above and below 57.5 °C.

In general, the unique texture dependence on the temperature is related to the growing kinetics, as both of them exhibit a discontinuous transition at the same temperature.

Packing and Interaction Difference. In Figure 6a is shown the ATR spectra in the 1450−750 cm^{-1} region of the PHP18Ks as prepared. The spectra of the pure β-form (PHP70K crystallized at 0 °C) and the pure γ-form (cast PHP70K) are included for a comparison. All the polymorphic samples show a similar IR absorption. To distinguish the bands of the crystalline phase from those of the amorphous phase, the time-resolved transmission FTIR spectra were registered during the crystallization of the PHP18Ks at various T_cs. In Figure 7a is shown one example, which is registered within the first 30 min after the initiation of the crystallization at 60 °C. Distinctively, the intensities of the bands at 1392, 1357, 1171, 1015, and 958 cm^{-1} escalate with the time elapsing, possibly reflecting some conformational rearrangements required for the crystallization.

The assignments of these solid bands were tentatively carried out on the basis of those by Wasai et al.[12] and by referring to those for polyethylene,[24] poly(ethylene glycol),[25,26] the related polyesters with ethylene glycol units,[27−34] and poly(ϵ-caprolactone).[35,36] The solid bands at 1391 and 1357 cm^{-1}, those at 1171 cm^{-1}, and those at 1015 and 958 cm^{-1} may correspond to the CH_2 wagging vibration, the C−O−C stretching mode, and the C−C stretching mode, respectively. It is well-known that these bands are very sensitive to the conformation of polymer chains either in the crystalline phase or in the amorphous phase. Thus, the similar infrared absorptions of these solid vibration modes again confirms that a similar chain conformation is adopted in both the β- and γ-form, i.e., the all-trans conformation.[11,13]

On the other hand, some small but distinctive spectral differences are also distinguished. In Figure 6b are shown the corresponding expanded ATR/IR spectra in the 1450−1400 and 820−780 cm^{-1} regions, which possibly reflect the CH_2 bending and the rocking vibration, respectively. Clearly, the β-form shows two singlet absorptions at 1427 and 801 cm^{-1}, while the γ-form exhibits two splitting pairs (1434, 1427 cm^{-1} and 806, 801 cm^{-1}). Moreover, the intensity of the 1434 or 806 cm^{-1} band decreases with the content of γ-form crystal relative to that of the 1427 or 801 cm^{-1} band. Thus, it seems that the two bands at 1434 and 806 cm^{-1} should be related to the γ-from while those at 1427 and 801 cm^{-1} to both the β- and γ-form crystals.

It is of interest to understand such IR absorption splitting. Normally, the IR is sensitive to the conformation and the intramolecular or intermolecular interactions of polymers. As discussed above, the polymer chains in the β- and γ-form crystals both adopt an all-trans conformation. In addition, the chains (along the c axis) in the γ-form are stretched more than those in the β-form.[13] Thus, the difference between the two crystals in the intermolecular interaction strength, i.e., the packing way, is the only possible reason for that in the IR absorption. In the case of polyethylene, the splitting of the CH_2 rocking absorption band at 720 cm^{-1} was considered to be the consequence of intermolecular interaction in the crystalline state.[24] In the γ-form of PHP, the chain setting angles with respect to the a axis of the corner and the center chains are ±51.5°, respec-

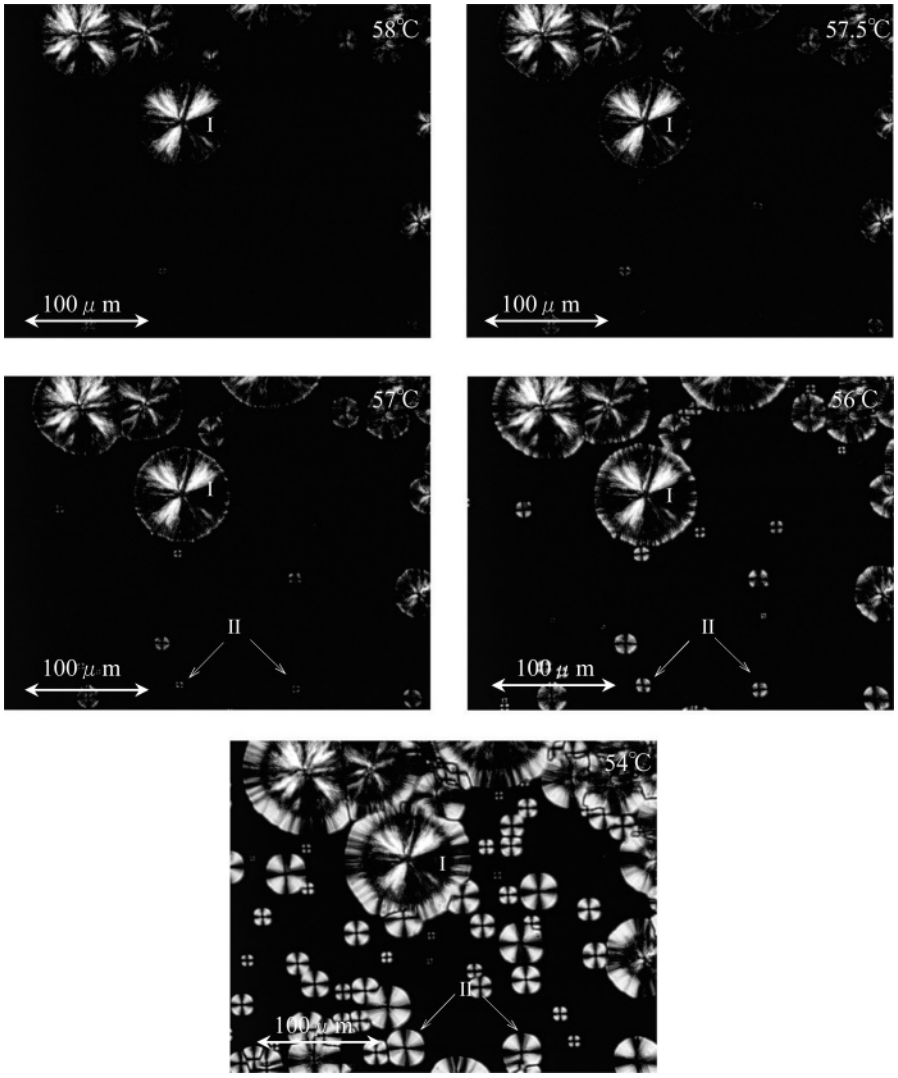

Figure 5. Optical microphotographs of spherulites in PHP23K cooled from 130 °C at 1 °C/min. I: spherulites growing above 57.5 °C, with a rough texture and a distorted Maltese cross. II: spherulites growing below 57.5 °C, with a smooth texture and a pronounced Maltese cross.

tively,[13] while in the β-crystal of PHP, the chain settingangles with respect to a axis is 0°,[11,13] which unambiguously indicates the tighter packing of the atoms in the γ-form along the a axis. The tighter packing of the atoms along the a axis would make atoms on the adjacent chains more strongly interacted, resulting in the corresponding IR absorption splitting. The crystal field splitting induced by the intermolecular interaction of neighboring chains is really few in polymer. The splitting pairs can be considered as "true" crystallinity bands, which can be used to detect the crystallization and crystalline structure directly. In addition, we also note that both crystals own a similar density, i.e., 1.42 and 1.44 g cm^{-3},[13,37] respectively, for the γ- and the β-form,[11] as the chains (along c axis) in the γ-form are stretched 3.2% more than those in the β-form.[11,13]

By employing a curve-fitting technique to analyze the FTIR spectra, it is found that the low wavenumber members of the splitting pair locate almost at the same frequency as those of the unperturbed mode in the pure β-form; i.e., they overlap with each other. Therefore, it is reasonable to assign the two bands at 1434 and 806 cm^{-1} to the γ-from and those at 1427 and 801 cm^{-1} to both the β- and γ-form crystals, which from now on are denoted as γ-bands and (β + γ)-bands, respectively. Thus, the intensity ratio between the paired components can unambiguously reflect the relative amounts of the two crystal forms in the crystalline phase, although possibly not as accurately as the corresponding area ratio obtained from the curve-fitting. It will be used to in-situ monitor the structure evolution during the crystallization and the melting because of the necessary high efficiency and reproducibility, as described later.

In Situ Observation on Polymorphic Crystallization. In parts a and b of Figure 7 are shown the time-resolved FTIR spectra of the PHP18K collected within the first 30 min after the initiation of the crystallization at 60 °C and their expanded figures, respectively. As was discussed above, the bands at 1392, 1357, 1171, 1015, and 958 cm^{-1} and the two splitting pairs, i.e., (1434, 1427 cm^{-1}) and (806 and 801 cm^{-1}), all originate from the crystalline phase of PHP, denoted as crystalline bands. On the other hand, the bands at 1261, 1171, and 1073 cm^{-1} are also sensitive to the crystallization, but their intensities decrease with time elapsing, suggesting they correspond to the vibration modes of amorphous chains, and are thus denoted as amorphous bands. Because of the direct correlation between the intensity of crystalline band and the crystallinity, the intensity change of crystalline bands will be followed to describe the crystallization kinetics

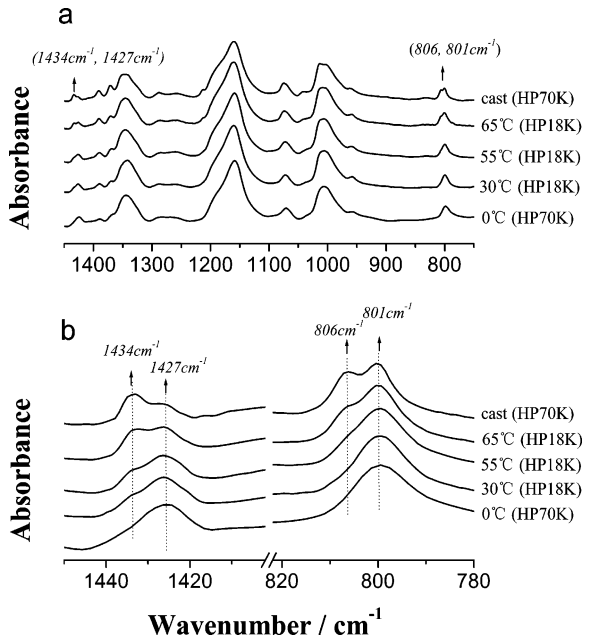

Figure 6. (a) ATR spectra in the 1450−750 cm^{-1} region for PHP70K melt-crystallized at 0 °C, PHP18Ks melt-crystallized at 30, 55, and 65 °C, and cast PHP70K. (b) Expanded figures in the 1450−1400 and 820−780 cm^{-1} regions.

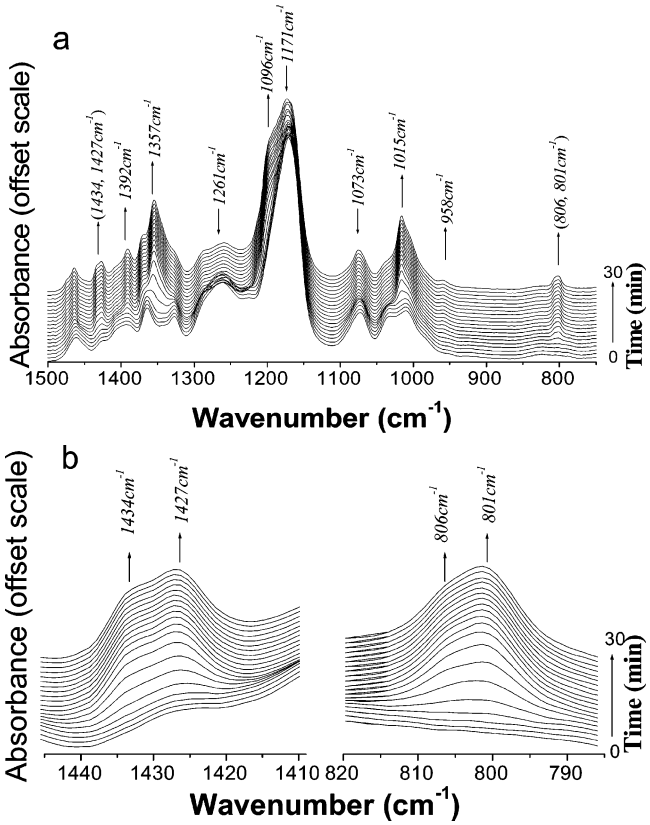

Figure 7. (a) Time-resolved FTIR spectra in the 1450−750 cm^{-1} range of PHP18Ks registered during the first 30 min crystallization at 60 °C. (b) Expanded figures in the 1450−1400 and 820−780 cm^{-1} regions. Bands indicated by "↑" and "↓" correspond to the crystalline and the amorphous ones, respectively.

and the subsequent melting. For the sake of clarity, a normalized intensity, H_s, is defined as $(H_t - H_0)/(H^s{}_\infty - H^s{}_0)$, where H_0 and H_t respectively represent the peak height of the specific band for the amorphous sample and that for the sample crystallized for a time of "t",

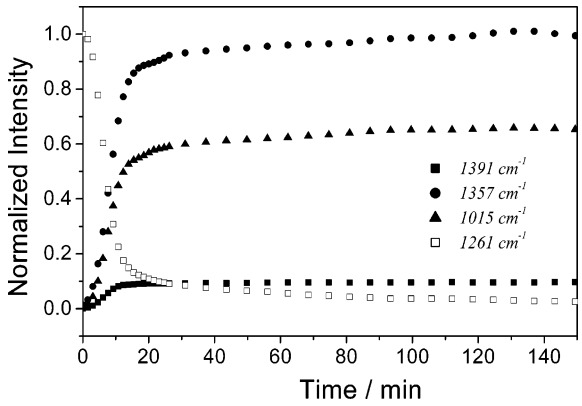

Figure 8. Normalized intensities of the crystalline (1391, 1357, 1015, and 1261 cm^{-1}) and the amorphous bands (1261 cm^{-1}) as a function of crystallization time for PHP18K at 60 °C.

while $H^s{}_0$ and $H^s{}_\infty$ denote respectively the peak height of the reference peak (normally, the band with the maximum height is selected as the reference to normalize the peak height) for the original sample and that after completion of crystallization. In Figure 8 are shown the plots of the normalized intensities of some crystalline bands at 1391, 1357, and 1015 cm^{-1} as a function of crystallization time for the PHP18K at 60 °C. For a clear comparison, the normalized intensity of the amorphous band at 1261 cm^{-1} is also included. Note that the intensities of crystalline bands increase with the crystallization time very rapidly during the first 40 min and henceforth slow down. Synchronously, the intensity of the amorphous band at 1261 cm^{-1} decreases gradually. The plots of normalized intensity for all bands against the crystallization time become almost flat after annealing the PHP18K at 60 °C for 120 min, indicating that the crystallization of PHP is basically completed during the first 120 min. Similar results are obtained for the PHP18K isothermally crystallized at other temperatures.

As shown in Figure 9a, the normalized intensities for the bands at 1434, 1427, 806, and 801 cm^{-1} are also plotted against the crystallization time for the PHP18K at 60 °C. The intensity ratios between the paired components of the two splitting pairs, $H^{1434}{}_s/H^{1427}{}_s$ and $H^{806}{}_s/H^{801}{}_s$, are plotted as a function of the crystallization time in Figure 9b. It is clear that both the intensity ratios are kept almost constant during the crystallization, besides some deviation or fluctuation at the earlier stage, suggesting that the chains are crystallized into the γ- and β-form crystal at a constant ratio during the whole crystallization process. Similarly, the intensity ratio is also calculated for the PHP18K crystallized at other temperature. In Figure 10 are shown the plot of the intensity ratios, $H^{1434}{}_s/H^{1427}{}_s$ and $H^{806}{}_s/H^{801}{}_s$, as a function of T_c. Obviously, both ratios decrease with decreasing T_c, indicating that the content of the γ-form crystal decreases with T_c, in good accordance with the X-ray analysis on the bulk samples.

In Situ Observation on Polymorphic Melting. To date, the different T_c is known to crystallize PHP chains into the polymorphic crystalline phases. The polymorphic melt-crystallized PHPs possibly show different melting behaviors during the subsequent heating. In parts a and b of Figure 11 are shown respectively the DSC thermograms at heating rates of 10 and 1 °C/min for the PHP18Ks melt-crystallized at the temperature ranging from 30 to 65 °C. As shown in Figure 11a, the

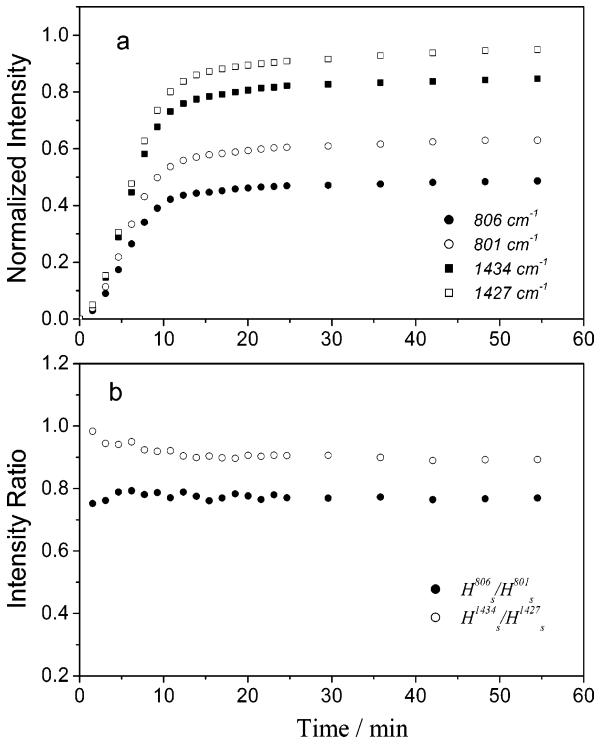

Figure 9. (a) Normalized intensities of polymorphism-sensitive bands at 1434, 1427, 806, and 801 cm^{-1} as a function of the crystallization time for PHP18Ks at 60 °C. (b) Intensity ratios between the paired components, i.e., $H^{1434}{}_s/H^{1427}{}_s$ and $H^{806}{}_s/H^{801}{}_s$, as a function of the crystallization time for PHP18K films at 60 °C.

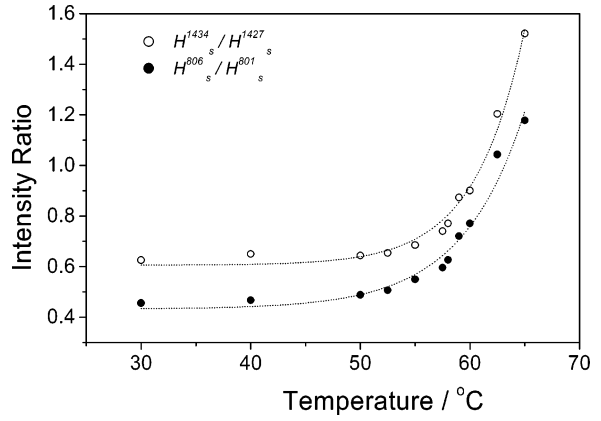

Figure 10. Intensity ratios between the paired components, i.e., $H^{1434}{}_s/H^{1427}{}_s$ and $H^{806}{}_s/H^{801}{}_s$, as a function of the crystallization temperature.

melt-crystallized PHP18Ks mainly exhibit three melting peaks, named $T_m{}^l$, $T_m{}^m$, and $T_m{}^h$ in the order of their positions. The T_c dependence for each melting peak is described below.

With increasing T_c, the melting enthalpy of $T_m{}^h$ increases, while its position remains almost constant. The position of $T_m{}^m$ shows a rather irregular dependence on T_c. With increasing T_c from 30 to 50 °C or from 60 to 65 °C, $T_m{}^m$ shifts upward. However, the increase of T_c from 50 to 60 °C results in a downshift of $T_m{}^m$. In addition, the position of $T_m{}^l$ is quite dependent on T_c, which is always 5−8 °C higher than T_c. It is clear that, except for $T_m{}^l$, the T_c dependences of $T_m{}^h$ and $T_m{}^m$ are not singular and are remarkable.

As is well-known, the multiple melting behaviors are a key to understanding the structural evolution during

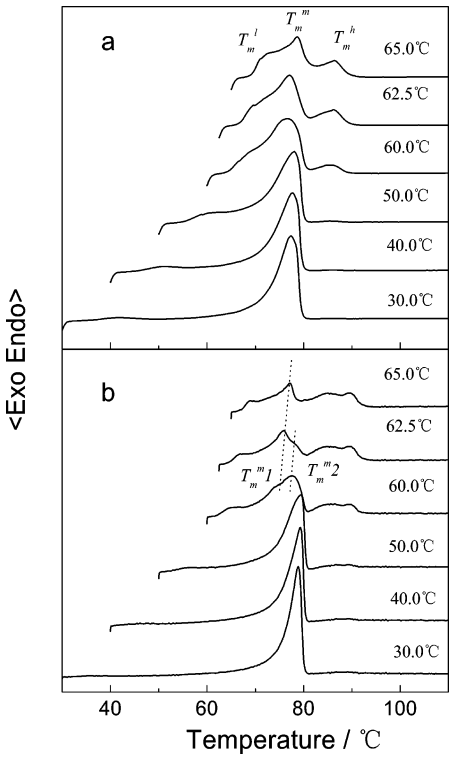

Figure 11. Melting thermograms of PHP18Ks melt-crystallized at various temperatures ranged from 35 to 65 °C at heating rates of (a) 10 and (b) 1 °C/min.

heating. A lot of effort has been made to clarify the multiple melting of polymers. The multiple melting behavior of polymer is normally attributed to the partial melting−recrystallization,[38] the crystals with different lamellar thickness,[39−42] or the crystals with different structures.[43,44] In the case of the polymorphic PHP, all the factors referred to above possibly control the melting of polymorphic PHPs, making it difficult to understand the multiple melting only relying on the DSC analyses. However, as the IR is very sensitive to the small changes of the conformation and the molecular environment in PHPs, our in-situ monitoring of the selected crystalline and polymorphism-sensitive bands is expected to shed light on the multiple melting of PHP.

The two γ-bands at 1434 and 806 cm^{-1} and the two $(\beta + \gamma)$-bands at 1427 and 801 cm^{-1} are also followed during the melting. In Figure 12 are shown the plots of the normalized intensities for the four bands as a function of the temperature, which were measured during the heating of HP18Ks crystallized at 30, 40, 50, 60, 62.5, and 65 °C, at a rate of 1 °C/min. For the sample crystallized at 65 °C, the normalized intensities of four bands exhibit the two-component exponential decay with heating. The inflection temperature between two exponential components corresponds to the initiation of the melting peak $T_m{}^h$. With decreasing T_c, the latter component is found to become weaker, corresponding to the weakened $T_m{}^h$.

To clarify the cause of the multiple melting, the decaying rate of the normalized intensity and the intensity ratio between the paired components of each splitting pair have been examined with the evolution of the temperature (T_e). Here, the decaying rate is defined as dH_s/dT_e. In Figure 13 are shown the decaying rates for the four bands plotted against the temperature. Obviously, the plots of decaying rate with the increased temperature are comparable to the corresponding DSC

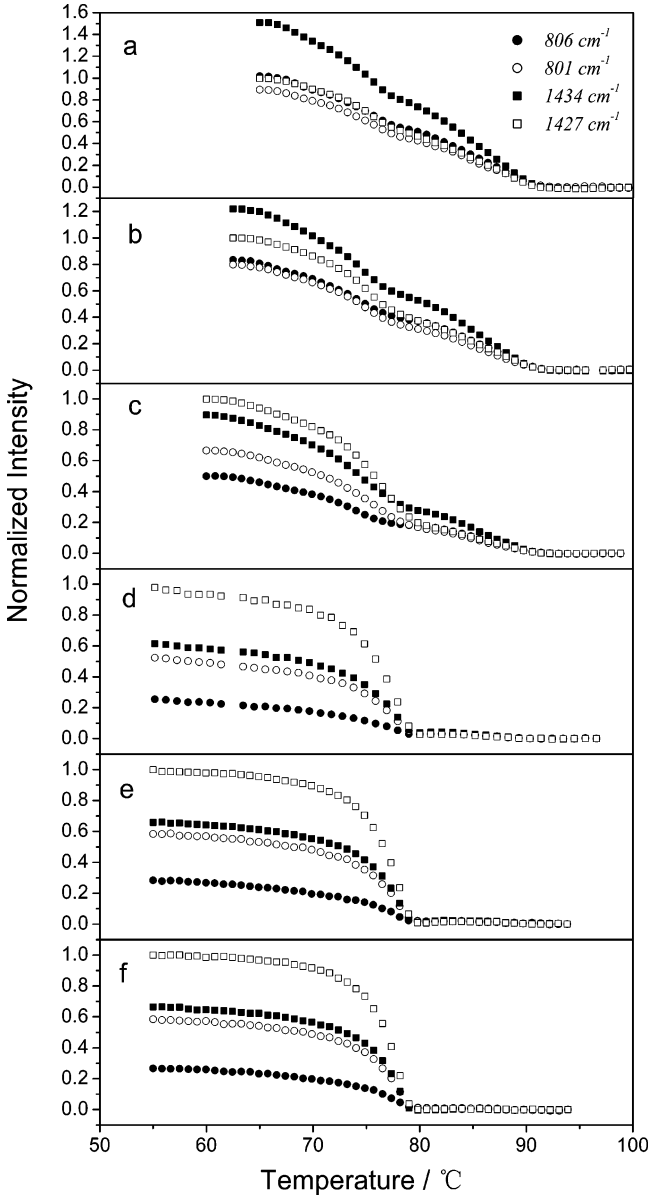

Figure 12. Normalized intensities of the polymorphism-sensitive bands at 1434, 1427, 806, and 801 cm^{-1} as a function of the temperature during the heating scan at a rate of 1 °C/min for HP18Ks melt-crystallized at (a) 65, (b) 62.5, (c) 60, (d) 50, (e) 40, and (f) 30 °C.

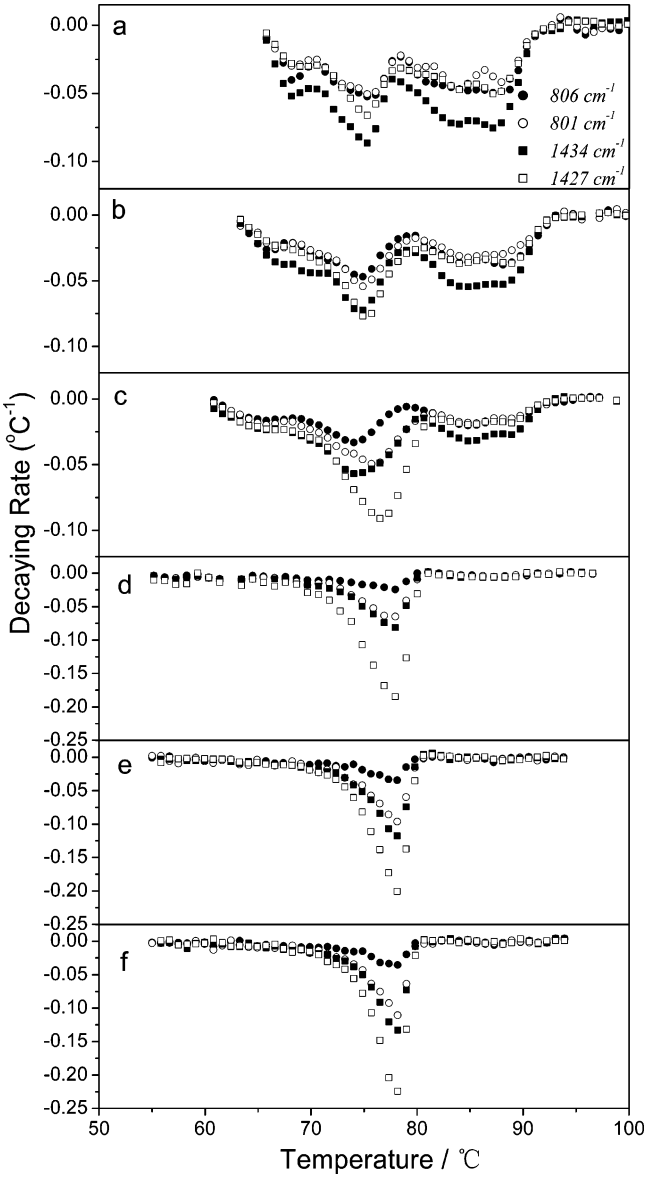

Figure 13. Decaying rates (intensity differential) of polymorphism-sensitive bands at 1434, 1427, 806, and 801 cm^{-1} as a function of the temperature during the heating scan at a rate of 1 °C/min for HP18Ks melt-crystallized at (a) 65, (b) 62.5, (c) 60, (d) 50, (e) 40, and (f) 30 °C.

heating scans. However, the plots of the decaying rate are used here to monitor not only the crystallinity but also the structural evolution of two form crystals during heating. For the PHP18Ks crystallized at 30, 40, 50, 62.5 and 65 °C, the decaying behavior of the γ-bands is similar to that of (β + γ)-bands. However, for the PHP18K crystallized at 60 °C, a difference of 2 °C has been found in the location of the maximum decaying rate. The two γ-bands show a maximum decaying rate at 75 °C, which is 2 °C lower than that of the two (β + γ)-bands. Does it suggest that the γ-form melts ahead of the β-form?

The intensity ratios between the γ-band and the (β + γ)-band, i.e., $H^{1434}{}_s/H^{1427}{}_s$ and $H^{806}{}_s/H^{801}{}_s$, are plotted against the temperature in Figure 14. Obviously, for the sample crystallized at 65 °C, $H^{1434}{}_s/H^{1427}{}_s$ and $H^{806}{}_s/H^{801}{}_s$ both exhibit a linear dependence on the increasing temperature. For the PHP18Ks crystallized at 50, 60, and 62.5 °C, besides an initial linear portion, the plots of $H^{1434}{}_s/H^{1427}{}_s$ and $H^{806}{}_s/H^{801}{}_s$ also show a subsequent jumping and soon leveling-off portion, indicating a rapid increase in the content of the γ-form occurs with heating, described as phase jumping. For the three samples, the phase jumping initiated at 77, 76, and 76 °C, respectively. For the PHP18Ks crystallized at 30 and 40 °C, the phase jumping could be observed if the enhanced error observed at above 78 °C caused by the much weakened intensity is ignored.

Discussion

The bimodal growth behavior shown in Figures 3 and 4 is possibly associated with the temperature-dependent polymorphism of PHP. However, there are also other cases where a polymer with a single form crystal also forms multiple morphologies and exhibits a corresponding multimodal growth behavior. The change of spherulite texture can arise from (i) that of the unit cell orientation with respect to the radius[45,46] or (ii) that of the chain-folding way (extended chains to folded ones

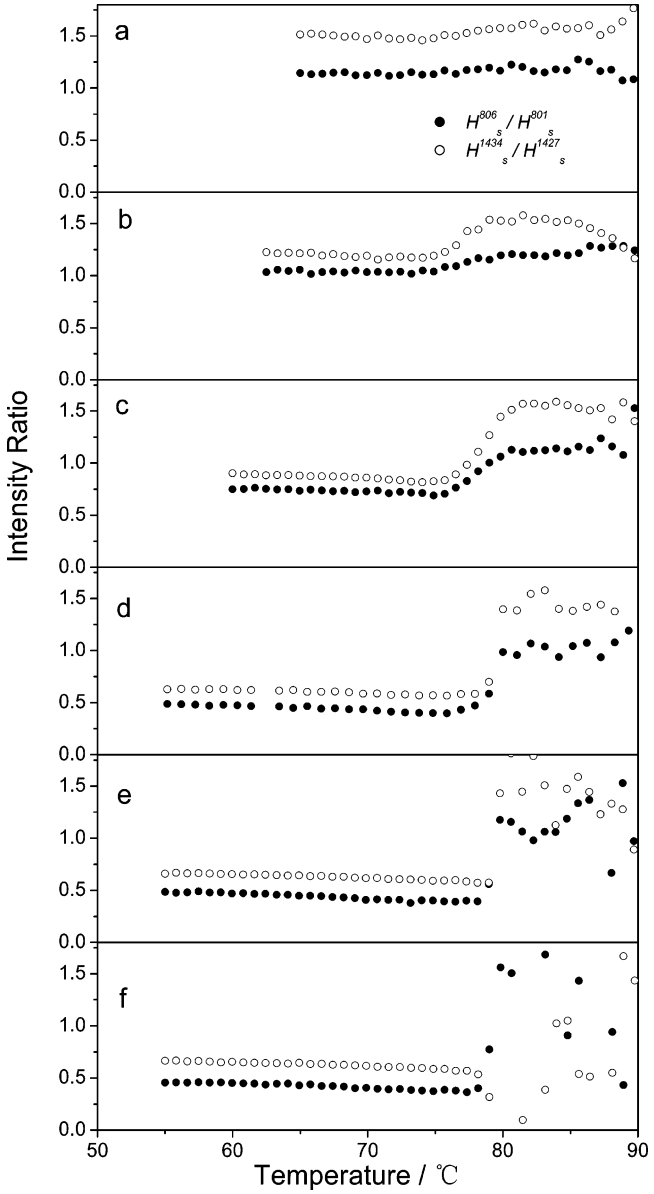

Figure 14. Intensity ratios between the paired components, i.e., $H^{1434}{}_s/H^{1427}{}_s$ and $H^{806}{}_s/H^{801}{}_s$, as a function of the temperature during the heating scan at a rate of 1 °C/min for HP18Ks melt-crystallized at (a) 65, (b) 62.5, (c) 60, (d) 50, (e) 40, and (f) 30 °C.

or nonintegral chain-folding to integral one).[47−49] Then, before drawing a conclusion, it is necessary to evaluate all the possible reasons. Normally, for a biaxial crystal (both the β- and γ-form of PHP are orthorhombic and biaxial), the unit cell orientation with respect to the radius decides the birefringence. The spherulite birefringence of PHP is found to persist in the 35−65 °C region, which thus intend to exclude the possibility of the origin (i). In addition, as investigated by SAXS, no temperature dependence can be detected for the crystal thickness (not shown), which also excludes the possibility of the origin (ii). As a result, the polymorphism is left as the most possible origin of the bimodal growth behavior.

How does the temperature-induced polymorphism affect the growth kinetics and the texture? Obviously, the spherulite structure is the key for answering this question. Unfortunately, the spherulite structure, especially the detailed spatially organizing way of the two crystal forms in one spherulite, is not clear yet. Then, we have to considering all the possible cases. Four pathways can realize the cogrowth of the two form crystals in one spherulite within the whole temperature region, i.e., (i) forming the respective lamellas, (ii) cocrystallizing in one lamella (in the macroscopic view, the alternating growth of the β- and the γ-form at a constant ratio could be constant), (iii) transforming from (i) to (ii) with the temperature increasing, and (iv) adopting the inverse way of (iii).

In the case of (i) and (ii), the growth rate equals to respectively that of the faster growing one and the value combining those of the two form crystals by considering their respective contribution. Obviously, at all events, without regarding the possible disturbance between their growths, the temperature-dependent polymorphism could result in the bimodal growth behavior, if the two form crystals have their own growth mode in very different temperature regions.

The spherulite texture much depends on the spatial organization of the two form crystals. In the cases of (i) and (ii), only one kind of spherulites occurs. In the cases of (iii) and (iv), two kinds of spherulites are possibly formed at above and below the critical temperature, which is well accordant with the discontinuous transition of the spherulite texture shown in Figure 5. With considering the remarkable depressed recrystallization of the γ-form in the β-rich phase (as discussed later), the possibility to adopt the case (iii) seems to be the most highest. Nevertheless, no instant driving force and direct evidence can be available until now, so we hesitate to draw a conclusion here. It still remains as a challenge to clarify the spatial organization of the two form crystals and is certainly of interest to us.

The temperature-induced polymorphism makes the melt-crystallized PHPs exhibit a complex melting behavior. As shown in Figure 11a,b, the location of $T_m{}^h$ is almost independent of T_c. With combining the results obtained by changing the heating rate (not shown), it is suggested that $T_m{}^h$ should correspond to the melting of the reorganized phases. Normally, the melting enthalpy of recrystallized phase should decrease with increasing T_c, as a more perfect crystalline phase can be obtained at higher T_c. However, as shown in Figure 11a,b, the intensity of the melting peak $T_m{}^h$ increases with increasing T_c.

With combining the time-resolved FTIR results, the melt-recrystallization phenomenon would be clarified. As shown in Figure 14b−d, during the heating of the PHP18Ks crystallized at 50, 60, and 62.5 °C, where an intense melting−crystallization occurs, the content of the γ-form crystals begins to increase at around 76 °C (about 4−5 °C lower than the melting of the recrystallized phase) and then level off within the melting range of the recrystallized phase. Two conclusions can be derived from these results: (i) The recrystallized phase is the γ- or γ-rich phase. (ii) A seeming phase jumping occurs with the melting. The phase jumping possibly arises from (i) the melt-recrystallization of the γ-from crystal. (iii) The $\beta \rightarrow \gamma$ transition induced by melt-recrystallization and/or (iv) the earlier melting of the β-form crystal. As shown in Figure 13b−d, all the results suggest that the γ-from crystal melt at lower temperature or at least at the same temperature with the β-from crystal (discussed later), excluding the possibility of the origin (iii). During the heating of the β-rich PHP18Ks (crystallized at 30 and 40 °C), no or weakened phase jumping, as indicated by the DSC and IR results,

occurs around 76 °C, eliminating the possibility of the origin (ii). Therefore, the origin of the phase jumping during melting should be only due to the melt-recrystallization of the γ-form crystal. The initiating temperature of the phase jumping should correspond to that of the melt-recrystallization. Consequently, it is reasonable to note that the amount of the recrystallized phase increases with T_c, then resulting in the enhanced peak intensity of $T_m{}^h$, as the content of the γ-form increases. In addition, as shown in Figure 14a−d, in the 50−65 °C region, the increase of T_c much enriches the γ-from crystals in the original phase but does not affect the content of the γ-form crystal in the recrystallized phase either (possibly indicating the recrystallize phase is a pure γ-form one). As a result, the difference in the content of the γ-form between the two phases becomes smaller, as indicated by the decreased "height" and even the almost elimination of the phase jumping with increasing T_c to 65 °C.

With regarding that a considerable amount of γ-form crystal does exist in the PHPs crystallized in the 30−50 °C region, as confirmed by Figure 1, the recrystallization of the γ-form crystal in the β-rich phase is likely to be excessively weakened, as shown in Figures 11−13, even without considering the normally stronger recrystallizability of the crystalline phase formed at the lower temperature. It seems some other factor also controls the recrystallization of the β-rich phase. As ever described, the two form crystals in the β-rich phase can cogrow in one lamella or not. The spatial organization of crystals would be related to the recrystallizability of the γ-form crystal. In the former case, the partially melted γ-form crystals are sandwiched between the unmelted β-form crystals, possibly results in the spatial restriction on their reorganization.

Besides the melting peak $T_m{}^h$, the γ-rich sample also shows two melting peaks at lower temperatures, that is, $T_m{}^m$ and $T_m{}^l$. No change of crystalline structure can be detected around the melting peaks of $T_m{}^l$. Possibly $T_m{}^l$ corresponds to the melting of thinner or imperfect crystals because of the low position and its distinctive dependence on T_c and the crystallization time (not shown). The main melting peak, $T_m{}^m$, should arise from the main crystalline phase, whose location and intensity quite depend on those of the recrystallization. For the β-rich samples crystallized in the 30−50 °C region, the weak recrystallization almost have no effects on the melting of the γ-from crystal, as indicated by Figure 13d−f. Namely, the intensities of the γ-bands and the (β + γ)-bands reach the maximum decaying rate at the same temperature. Once is T_c increased to above 50 °C, the recrystallization of the γ-from crystal is sharply enhanced, resulting in the unique downshift of $T_m{}^m$ with the increase of T_c. Considering the temperature dependence of polymorphism for PHP is continuous, as discussed such a sharp enhancement of the recrystallization possibly arises from the alteration of the spatial organization way of the crystalline phase. As a result, the much enhanced recrystallization would shift the melting point of the γ-form crystal to be lower than that of the β-form crystal, as experienced by the sample crystallized at 60 °C and shown in Figure 13c. It is clear that the intensity of the γ-bands and the (β + γ)-bands reach the maximum decaying rate respectively at 75 and 77 °C. Correspondingly, $T_m{}^m$ splits into $T_m{}^m1$ (75 °C) and $T_m{}^m2$ (77 °C) in the DSC heating scan, as shown in Figure 12b. With increasing T_c, the contribution of the β-form to the (β + γ)-bands becomes weaker, thus making the decaying behavior of the (β + γ)-bands and the γ-bands similar to each other, as shown in Figure 13a,b. However, the DSC heating scans still hold the sensitivity to the melting of the β-form crystal. As shown in Figure 12b, the reduction of the amount of β-form would result in the much smaller $T_m{}^2$ and even the absence of $T_m{}^2$ during the melting of the samples crystallized at 62.5 and 65 °C, respectively.

In addition, the seeming previous melting of the γ-form does not necessarily indicate that the β-form is more thermodynamically stable than the γ-form. To compare the thermodynamic stabilities of the two crystals, it is necessary to understand the differences in the equilibrium melting point ($T_m°$) of PHP polymorphs. However, the strong effects of the melt-recrystallization on the melting behavior of the γ-form and the difficulty to prepare the pure crystalline phase make the accurate determination of $T_m°$ unpractical. Nevertheless, the linear Hoffman−Weeks extrapolation is still applied here to estimate approximately the equilibrium melting point. The equilibrium melting point of the β-form and that of the γ-form are determined to be respectively 81.2 and 104.9 °C, suggesting that the γ-form is more thermally stable. However, no phase transition from the β-crystal to the γ-from can be detected.

Conclusion

In PHPs, the formation of the γ-form crystal was found to be thermodynamically favored at higher T_c, while the β-form crystal is kinetically favored at lower T_c. Furthermore, the PHPs with higher molecular weight more readily crystallize into the γ-form crystal. The temperature-induced polymorphism leads to the bimodal spherulite growth behavior, which occurs along with a discontinuous temperature dependence of the morphology. Similar to previous works but independent on their methods, PHP chains in the γ- and the β-form are found to adopt a similar conformation, but those in the γ-form are possibly packed more tightly along the a axis, resulting in the crystal field splitting.

The corresponding IR absorption splitting distinguishes the γ-form from the β-form, which endows the IR with the capability to detect the structure evolution during the crystallization and the melting. It is found that the β- and γ-form crystals cogrow in one spherulite at a constant ratio, promising the constant growth. During the melting, only the γ-form crystal can be reorganized into the perfect crystalline phase. The recrystallized phase possibly contains the γ-form crystal only. The recrystallization of the γ-form crystal downshifts the melting of the γ-from crystal and leads to the split melting of the γ-rich sample.

References and Notes

(1) Doi, Y. In *Microbial Polyesters*; VCH Publishers: New York, 1990.
(2) Inoue, Y.; Yoshie, N. *Prog. Polym. Sci.* **1992**, *17*, 571.
(3) Yoshie, N.; Inoue, Y. In *Biopolymers*; Steinbüchel, A., Doi, Y., Eds.; Wiley-VCH: Weinheim, 2001; Vol. 3, Chapter VI.
(4) Brophy, M. R.; Deasy, P. B. *Int. J. Pharm.* **1986**, *29*, 223.
(5) Juni, K.; Nakano, M.; Kubota, M. *J. Controlled Release* **1986**, *4*, 25.
(6) Akhtar, S.; Pouton, C. W.; Notarianni, L. J. *Polymer* **1992**, *33*, 117.
(7) Iwata, T.; Aoyagi, Y.; Fujita, M.; Yamane, H.; Doi, Y.; Suzuki, Y.; Takeuchi, A.; Uesugi, K. *Macromol. Rapid Commun.* **2004**, *25*, 1100.

(8) Orts, W. J.; Marchessault, R. H.; Bluhm, T. L.; Hamer, G. K. *Macromolecules* **1990**, *23*, 5368.
(9) Eling, W. B.; Gogolewski, S.; Pennings, A. J. *Polymer* **1982**, *23*, 1587.
(10) Hoogsteen, W.; Postema, A. R.; Pennings, A. J.; Ten Brinke, G.; Zugenmaier, P. *Macromolecules* **1990**, *23*, 634.
(11) Suehiro, K.; Chatani, Y.; Tadokoro, H. *Polym. J.* **1975**, *7*, 352.
(12) Wasai, T.; Saegusa, T.; Furukawa, J. *Kogyo Kagaku Zasshi* (*J. Chem. Soc. Jpn., Ind. Chem. Sect.*) **1964**, *67*, 601.
(13) Furuhashi, Y.; Iwata, T.; Sikorski, P.; Atkins, E.; Doi, Y. *Macromolecules* **2000**, *33*, 9423.
(14) Furuhashi, Y.; Iwata, T.; Yoshiharu, K.; Doi, Y. *Macromol. Biosci.* **2003**, *3*, 462.
(15) Cornibert, J.; Marchessault, R. H. *Macromolecules* **1975**, *8*, 296.
(16) Cornibert, J. Ph.D. Thesis, Université de Montréal, 1972.
(17) Zhu, B.; He, Y.; Asakawa, N.; Yoshie, N.; Nishida, H.; Inoue, Y. *Macromol. Rapid Commun.* **2005**, *26*, 581.
(18) Chen, M.; Chung, C. T. *J. Polym. Sci., Polym. Phys. Ed.* **1998**, *36*, 2393.
(19) Ritcey, A. M.; Prud'homme, R. E. *Macromolecules* **1992**, *25*, 972.
(20) Hoffman, J. D.; Davis, G. T.; Lauritzen, J. L. In *Treatise on Solid State Chemistry*; Hanny, N. B., Ed.; Plenum Press: New York, 1976.
(21) Hoffman, J. D. *Polymer* **1983**, *24*, 3.
(22) Di Lorenzo, M. L.; Cimmino, S.; Silvestre, C. *Macromolecules* **2000**, *33*, 3828.
(23) Di Lorenzo, M. L. *Polymer* **2001**, *42*, 9441.
(24) Krimm, S.; Liang, C. Y.; Sutherland, G. B. B. M. *J. Chem. Phys.* **1956**, *25*, 549.
(25) Matsuura, H.; Miyazawa, T. *J. Polym. Sci.* **1969**, *7*, 1735.
(26) Li, X.; Hsu, S. L. *J. Polym. Sci., Part B* **1984**, *22*, 1331.
(27) Quchi, I.; Hosoi, M.; Shimotsuma, S. *J. Appl. Polym. Sci.* **1977**, *21*, 3445.
(28) Kimura, F.; Kimura, T.; Sugisaki, A.; Komatsu, M.; Sata, H.; Ito, E. *J. Polym. Sci., Polym. Phys. Ed.* **1997**, *35*, 2741.
(29) Vasanthan, N.; Salem, D. R. *Macromolecules* **1999**, *32*, 6319.
(30) Ward, I. M. *Chem. Ind. (London)* **1956**, 905.
(31) Ward, I. M. *Chem. Ind. (London)* **1957**, 1102.
(32) Miyake, A. *J. Polym. Sci.* **1959**, *38*, 479.
(33) D'Espositio, L.; Koenig, J. L. *J. Polym. Sci., Polym. Phys. Ed.* **1976**, *14*, 1731.
(34) Lin, S.-B.; Koenig, J. L. *J. Polym. Sci., Polym. Phys. Ed.* **1982**, *20*, 2277.
(35) Holland-Moritz, K.; Hummel, D.-O. *J. Mol. Struct.* **1973**, *19*, 289.
(36) Holland-Moritz, K.; Siesler, H.-W. *Appl. Spectrosc. Rev.* **1976**, *11*, 1.
(37) Grescenzi, V.; Manzini, G.; Calzolari, G.; Borri, C. *Eur. Polym. J.* **1972**, *8*, 449.
(38) Al-Hussein, M.; Strobl, G. *Eur. Phys. J. E* **2001**, *6*, 305.
(39) Denchev, Z.; Nogales, A.; Sics, I.; Ezquerra, T. A.; Balta-Calleja, F. J. *J. Polym. Sci., Polym. Phys. Ed.* **2001**, *39*, 881.
(40) Hsiao, B. S.; Wang, Z.; Yeh, F.; Gao, Y.; Sheth, K. C. *Polymer* **1999**, *40*, 3515.
(41) Verma, R.; Marand, H.; Hsiao, B. *Macromolecules* **1996**, *29*, 7767.
(42) Verma, R. K.; Hsiao, B. S. *Trends Polym. Sci.* **1996**, *4*, 312.
(43) Ho, R. M.; Lin, C. P.; Tsai, H. Y.; Woo, E. M. *Macromolecules* **2000**, *33*, 6517.
(44) Sun, Y. S.; Woo, E. M. *Macromolecules* **1999**, *32*, 7836.
(45) Bunn, C. W.; Garner, E. V. *Proc. R. Soc. London A* **1947**, *189*, 39.
(46) Lovinger, A. J. *J. Appl. Phys.* **1978**, *49*, 5003.
(47) Organ, S. J.; Ungar, G.; Keller, A. *Macromolecules* **1989**, *22*, 1995.
(48) Cheng, S. Z. D.; Lotz, B. *Philos. Trans. R. Soc. London A* **2003**, *361*, 517.
(49) Fu, Q.; Heck, B.; Strobl, G.; Thomann, T. *Macromolecules* **2001**, *34*, 2502.

MA050534Q